ARMY RESEARCH LABORATORY

A Technique to Ease the Fabrication Tolerance of Integrated Optical Power Splitters

by Tristan J. Tayag and David M. Mackie

ARL-TR-1517

February 1998

Army Research Laboratory
Adelphi, MD 20783-1197

ARL-TR-1517 **February 1998**

A Technique to Ease the Fabrication Tolerance of Integrated Optical Power Splitters

Tristan J. Tayag
Texas Christian University

David M. Mackie
Sensors and Electron Devices Directorate, ARL

Abstract

Fabrication tolerances and sidewall scattering losses in self-imaging waveguide devices are ameliorated by a partial-etch fabrication technique. Using a modal decomposition model, we find that the self-imaging plane's depth of focus increases with a reduction in etch depth. A broad depth of focus in the self-image plane relaxes the fabrication tolerance of the device's critical width dimension for a specified device performance. Trade-offs for this increased depth of focus include a modest increase in device length and a slight reduction in peak coupling efficiency.

Contents

Figures

1. Introduction

Research is under way at the Communications and Electronics Command (CECOM) and the Army Research Laboratory (ARL) in the development of integrated photonic subsystems (IPSs) for use in the optical control of phased-array antennas for communications on the move. Figure 1 shows a block diagram of the phased-array controller. In the figure, the module labeled IPS 2 provides the first level of signal splitting required to feed the antenna, which might vary from hundreds to thousands of elements. ARL is developing optical power-splitting devices to be used in IPS 2.

Desired characteristics of a $1 \times N$ splitter for this application include a value for N of about 16, the ability to split both the transverse electric (TE) and transverse magnetic (TM) modes, low crosstalk between the two polarization modes, uniformity among the split channels, low throughput loss, compact size, and ease of manufacture. For $N > 4$, fiber-optic polarization preserving splitters are impracticable. Therefore, the splitting must be performed on an integrated optical substrate. Numerous passive integrated optical beamsplitting techniques have been proposed and demonstrated. These include but are not limited to Y-junction branching waveguides, evanescent field directional couplers, computer-generated waveguide holograms, multimode interference (MMI) splitters, and radiative power splitters. For achieving the desired device characteristics, the MMI approach holds the greatest promise.

The practical implementation of MMI devices in guided-wave architectures largely depends on the device's fabrication tolerance, as defined by such performance metrics as excess optical loss. Using the paraxial approximation for strongly guided (i.e., deeply etched) structures, Besse et al [1] derived a closed-form approximation for the critical width dimension of the MMI region. For these deeply etched devices, they found that the fabrication tolerance is independent of the splitting ratio N and proportional to the output channel separation D.

A partial or shallow etch of the MMI device, however, is advantageous in many devices. For example, reduced sidewall interaction results in lower

Figure 1. Architecture for optical phased-array antenna control. Architecture is subdivided into four integrated photonic subsystems (IPSs).

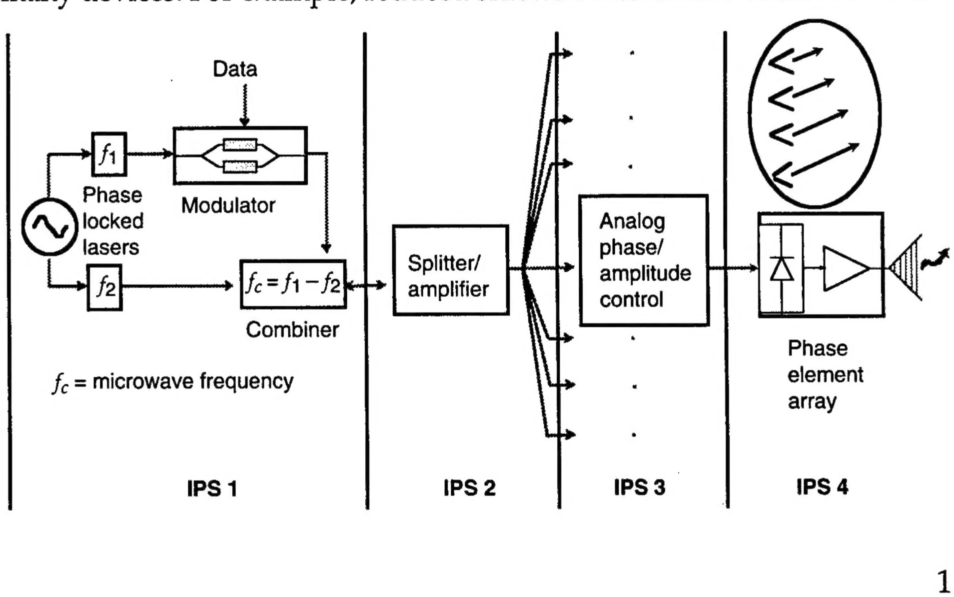

excess loss and decreased nonradiative surface recombination in waveguide ring lasers [2]. Berry and Burke [3] used the discrete spectral index method to predict the self-imaging length and throughput of MMI devices as a function of etch depth. Shortly thereafter, 1×16 splitters with high throughput and good uniformity were demonstrated that were built by the partial-etch technique [4].

Since MMI devices are based on the principle of Talbot imaging (also known as self-imaging), the imaging plane's depth of focus can significantly affect the device fabrication tolerance. Recently, Smit et al [5] reported an increase in image plane focal depth with an increase in input rib width for deeply etched structures. In addition, excess loss was reduced, since a smaller fraction of the signal was contained in the higher order modes.

In this report, we review the results of a theoretical investigation of the depth of focus dependence on etch depth in MMI devices. We find that a shallow etch depth yields an extended depth of focus and thus a broader fabrication tolerance, at the expense of a slight penalty in throughput. This throughput loss results from a reduction in the number of modes supported within the MMI region, and we show that this loss is negligible for etch depths beyond mode cutoff.

2. Theory

Since a 1 × 1 MMI device produces a single self-image of the input, this configuration (fig. 2) is the simplest for investigating the effect of etch depth on imaging plane depth of focus. We make the following assumptions concerning the MMI structure under investigation (fig. 2): (1) the depth of focus is analyzed at the first single self-image plane, (2) the input rib, MMI region, and output rib are all defined in a single etch step, and (3) the device sidewalls are vertical.

Figure 3 shows the refractive index and thickness values used to define the transverse waveguide structure. These values correspond to an InGaAs/InAlAs waveguide operating at 1.319 μm. Although these parameters vary from one waveguide structure to the next, our analysis is presented in terms of mode index difference between the MMI region and the surrounding etched regions; this approach allows us to generalize to other structures.

The etch depth of those areas surrounding the MMI region determines the mode index difference. Together with the MMI region width, this index difference determines the number of lateral modes supported within the MMI region. These modes will be excited to varying degrees by an input to the MMI region. Since each mode propagates with a slightly different phase velocity, the modes become dephased. At the place where the accumulated phased differences among the modes reach an integral multiple of 2π, a self-image of the input to the MMI region is reconstructed; i.e., the image is created solely by virtue of diffraction. No optical elements are required.

To reduce the three-dimensional structure of figure 2 to a two-dimensional structure, we have modeled the self-image formation by

Figure 2. Perspective view of a 1 × 1 multimode interference device.

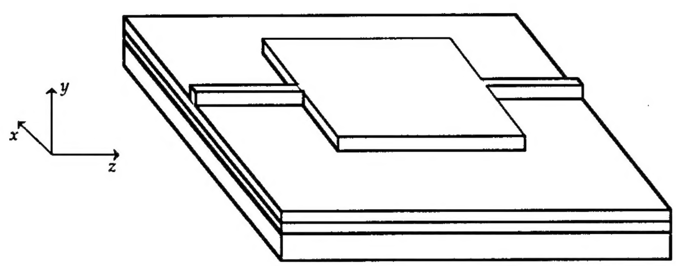

Figure 3. Transverse waveguide structure with film indices and thickness at 1.319 μm: cross section through MMI region.

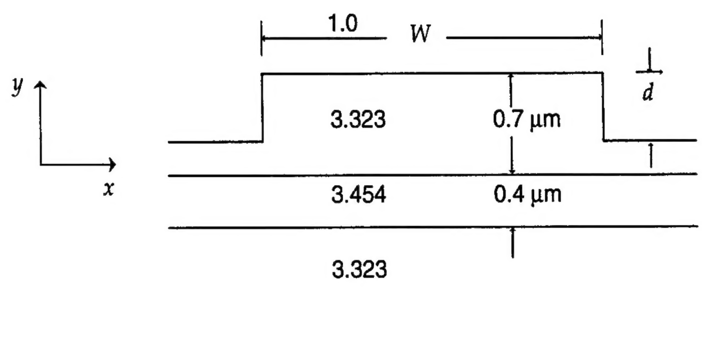

using the effective index method along the transverse waveguide dimension. The lateral modes of the MMI region are then calculated. The rib waveguide mode is decomposed into these lateral MMI modes (which are propagated the length of the MMI region), and the self-image is constructed [6,7]. As the etch depth is increased, a greater number of lateral modes are supported, not only in the MMI region, but also in the input rib waveguide. However, in our calculations, we assume that only the fundamental mode of the input rib waveguide is excited.

3. Results

The gray-scale contour plots of the MMI region's electric field amplitude (fig. 4) show the field evolution through the MMI region for three characteristic etch depths: very shallow, at mode cutoff, and very deep. The input rib width is fixed at 2 μm, and the MMI region width is fixed at 10 μm for each of the etch depths. Two points are immediately apparent from figure 4. First, the MMI region's self-imaging length is longer for shallow etch depths; second, the depth of focus and input field width are greater with shallower etch depths. These observations of a waveguide self-imaging system parallel the general behavior of a single-lens imaging system. For a fixed aperture size, as the imaging distance is increased, both the depth of focus and the focused spot size are increased [8].

Berry and Burke [3] used the discrete spectral index method to predict the position of the self-imaging plane as a function of etch depth. Our results, based on the effective index method and modal propagation, corroborate their findings. The increase in self-imaging plane length with decreasing etch depth can be attributed to the *effective* width of the MMI region. The

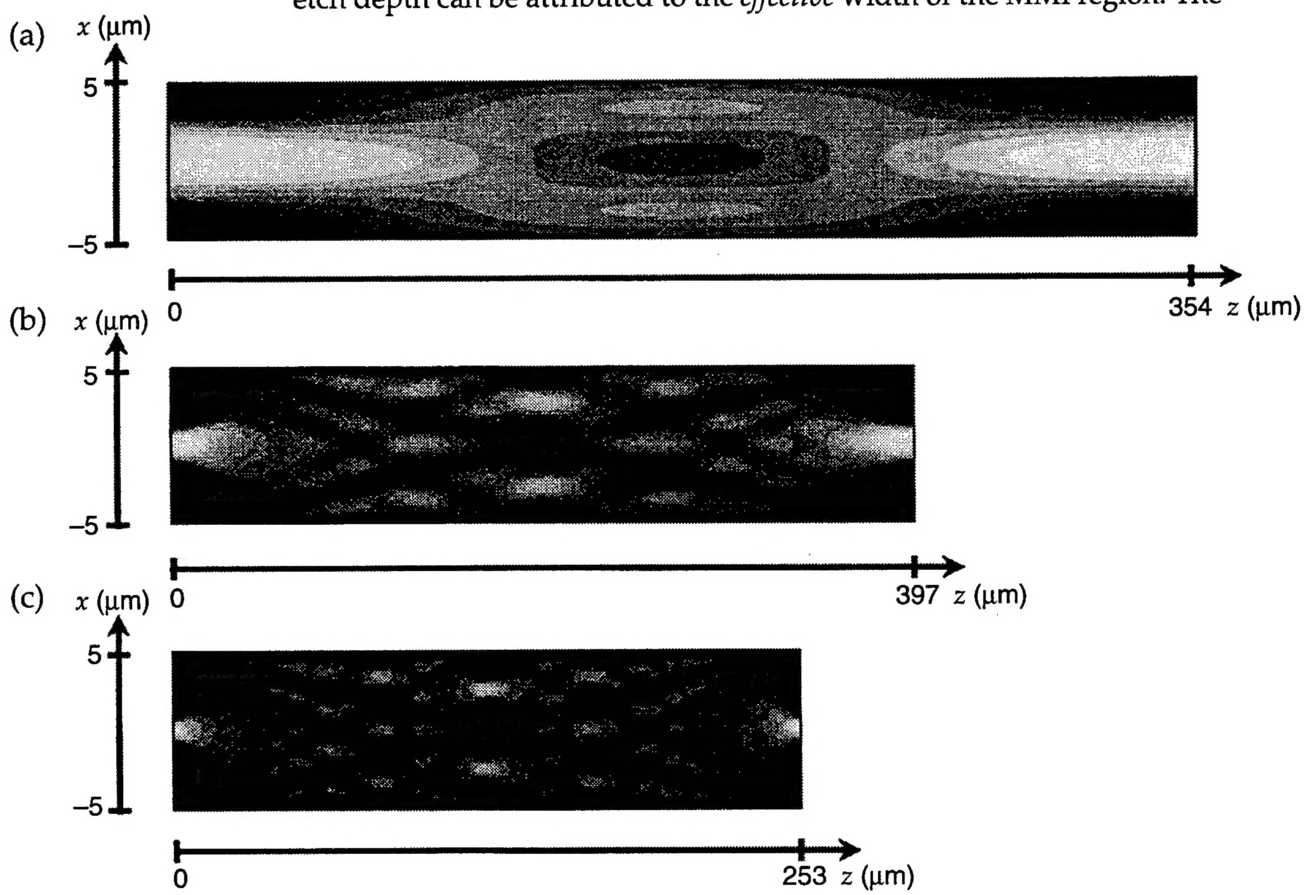

Figure 4. Top view of MMI region showing a gray-scale plot of TE field. (a) Etch depth 0.52 μm; only 3 lateral modes supported in MMI region. (b) Etch depth 0.82 μm (transverse mode is at cutoff); 10 lateral modes supported in MMI region. (c) Semi-infinite etch depth assumed (i.e., lateral mode index surrounding MMI region and input/output rib waveguides is unity); 49 lateral modes supported in MMI region.

effective width W_e is equal to the MMI region's physical width W, corrected by the Goos-Hänchen penetration depth [9]:

$$W_e = W + \left(\frac{\lambda}{\pi}\right)\left(\frac{n_{lat}}{n_{mmi}}\right)^{2\sigma}\frac{1}{\sqrt{n_{mmi}^2 - n_{lat}^2}} , \tag{1}$$

where λ is the free space wavelength, n_{lat} and n_{mmi} are the transverse mode indices of the lateral (etched) and MMI (unetched) regions, respectively, $\sigma = 0$ for TE polarization, and $\sigma = 1$ for TM polarization. In this expression, we assigned a fixed effective width for all the lateral modes in the MMI region. (Our actual analysis is more rigorous.) Given this etch-depth–dependent effective width, the self-image plane positions of a $1 \times N$ center-fed MMI coupler are approximated by [10]

$$L \cong \frac{n_{mmi}\, W_e^2}{N\lambda}. \tag{2}$$

The analytical approximations of equations (1) and (2) are in good agreement with the more exact modal propagation analysis of the self-imaging length's etch-depth dependence (see fig. 5). As the MMI region width is increased, however, the analytical approximation breaks down.

The efficacy of MMI devices in photonic switching systems is contingent on the relative ease in fabricating high-throughput devices. The imaging plane depth of focus determines the fabrication tolerance on the MMI region's critical width dimension. In this report, we use the coupling efficiency from the self-image formed at the end of the MMI region into the output rib as the defining metric for depth of focus. We calculate the coupling efficiency by performing an overlap integral of the MMI field with the mode supported by the output rib. This efficiency is converted to excess device loss.

In figure 6, we plot the depth of focus (assuming a maximum permissible excess loss of 1 dB) versus the mode index difference between the MMI and lateral regions for TE polarization. For mode index differences less than that corresponding to mode cutoff in the lateral region, the depth of focus varies rapidly with mode index difference.

In figure 7, we used the effective index method to plot the depth of focus versus etch depth for depths down to mode cutoff. In the limit of a very deep etch, the effective index of the lateral region approaches unity, yielding an asymptotic limit for the depth of focus. We can approximate the MMI device fabrication tolerance by differentiating equation (2) with respect to the physical device width W and rearranging:

$$\Delta W = \frac{N\lambda\, \Delta L}{2n_{mmi}\, W_e}. \tag{3}$$

For our test structure, a deep etch yields a depth of focus of about 12 μm, which requires a tolerance of ±0.12 μm in the MMI region width. At mode cutoff, the depth of focus is increased to about 28 μm, for a more easily manufacturable MMI width tolerance of ±0.26 μm.

Figure 5. Comparison of 1×1 self-imaging lengths as a function of etch depth for modal propagation and approximate analytical solutions.

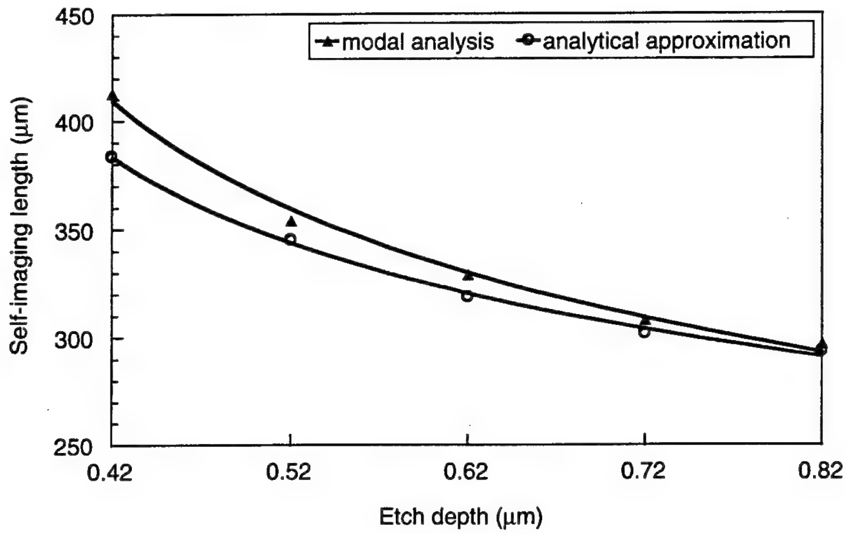

Figure 6. Depth of focus versus mode index difference between MMI region and surrounding etched regions. Depth of focus is determined at an excess coupling loss of 1 dB.

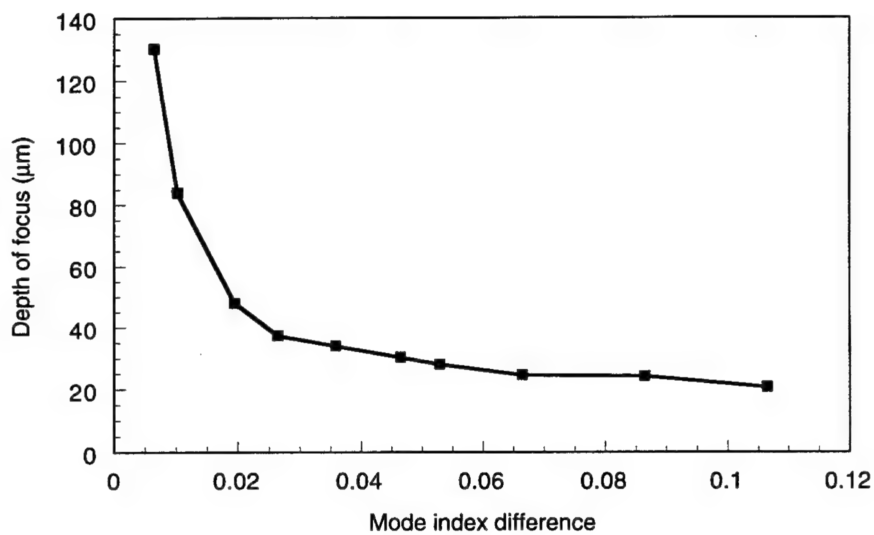

Figure 7. Depth of focus versus etch depth obtained by effective index method. Depth of focus is determined at an excess coupling loss of 1 dB. For a semi-infinite etch depth, depth of focus asymptotically approaches 12 μm.

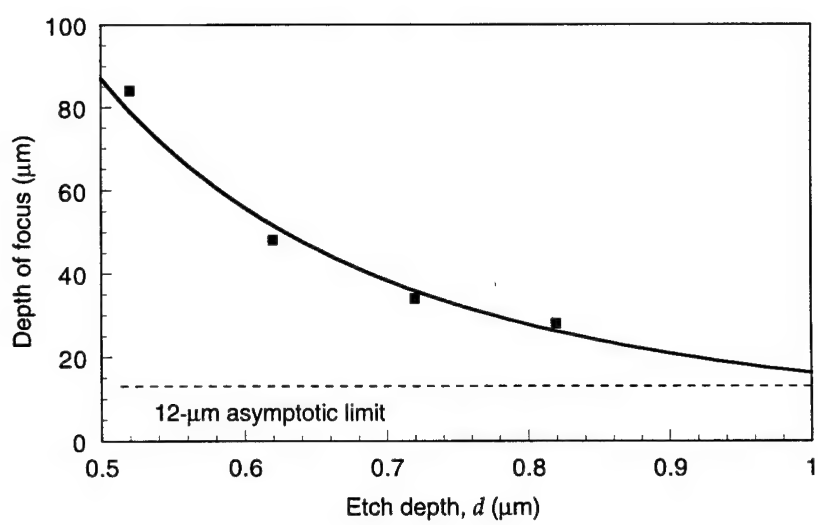

Although the data presented here correspond to the specific structure selected, the basic trend of an increased depth of focus (and thus fabrication tolerance with a decreased etch depth) is generalizable to arbitrary waveguide structures. As shown in figure 4, the shallower etch depths produce a broader fundamental mode in the fixed 2-μm-wide input rib. This extended depth of focus with a laterally wider input field is consistent with the findings of Smit et al [5], who investigated extending the depth of focus for deeply etched MMI devices by increasing the physical width of the input rib.

Several drawbacks arise from a reduced MMI device etch depth. We have already characterized the increase in device length due to the broader effective width as given by equations (1) and (2). Next, the etch depth affects self-image quality. With a smaller mode index difference between the MMI and laterally etched regions, fewer lateral modes are available for reconstructing the input for self-image formation. The consequence of the distorted image is to reduce the coupling efficiency into the output rib. However, figure 8 shows that a reduction in peak coupling efficiency from the distorted image into the output rib is negligible for etch depths to mode cutoff or greater. Finally, a shallower etch depth in the *N* output ribs requires a larger output rib separation to avoid mutual coupling among the ribs. If the output rib separation is accomplished with waveguide S-bends, a larger radius of curvature is required, because of the weaker mode confinement.

Figure 8. Maximum coupling efficiency of self-image into output rib waveguide as a function of etch depth. Transverse mode is cut off at etch depth of 0.82 μm.

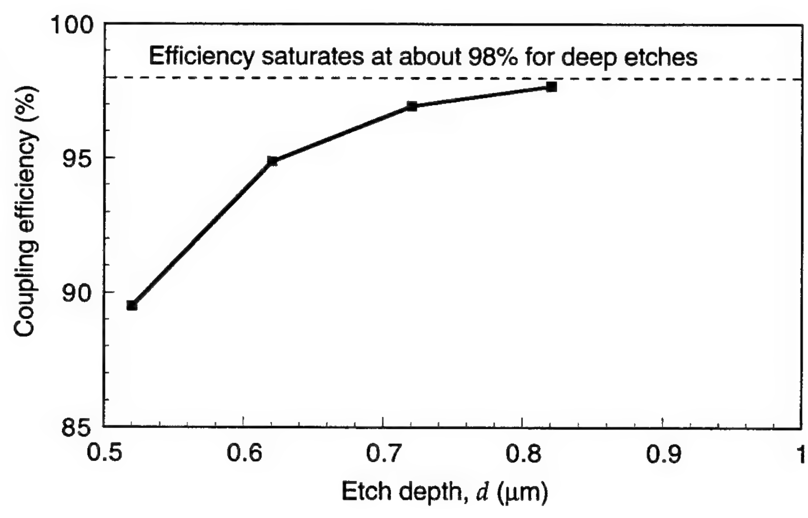

4. Conclusions

The etch depth in MMI device fabrication is a design variable that can be exploited to improve device manufacturability. In the 1×1 test structure, our model predicted a doubling of the MMI width fabrication tolerance when the MMI device is etched to a depth where the transverse waveguide mode is just cut off, as opposed to the deep etches that are typically used. This doubling is accomplished through an increase in the image plane depth of focus. The concomitant distortion of the self-image is negligible for etches to mode cutoff or deeper. These advantages to varying the MMI device etch depth are traded off with an increase in device length and weaker confinement in the modes of the output rib array.

References

1. P. A. Besse, M. Bachmann, H. Melchior, L. B. Soldano, and M. K. Smit, "Optical bandwidth and fabrication tolerances of multimode interference couplers," *J. Lightwave Technol.* **12**, no. 6, 1004–1009, 1994.

2. T. Krauss, R. M. Delarue, I. Gontijo, and P.J.R. Laybourn, "Strip-loaded semiconductor ring lasers employing multimode interference output couplers," *Appl. Phys. Lett.* **64**, no. 21, 2788–2790, 1994.

3. G. M. Berry and S. V. Burke, "Analysis of optical rib self-imaging multimode interference (MMI) waveguide devices using the discrete spectral index method," *Opt. Quantum Electron.* **27**, 921–934, 1995.

4. T. J. Tayag, D. M. Mackie, and G. W. Bryant, "A manufacturable technique for implementing low-loss self-imaging waveguide beamsplitters," *IEEE Photon. Technol. Lett.* **7**, no. 8, 896–898, 1995.

5. M. K. Smit, C.G.M. Vreeburg, and L. H. Spiekman, "Compact components for semiconductor photonic switches," *1996 Internat. Meeting on Photonics in Switching Tech. Dig.* (IEICE, Japan), Vol. 1, pp 74–75, 1996.

6. D. M. Mackie, T. J. Tayag, and G. W. Bryant, "Modeling of self-imaging integrated optical power splitters," *Proc. Fifth Biennial DoD Photon. Conf.* (AFCEA, Fairfax, VA), pp 59–64, 1996.

7. L. B. Soldano and E.C.M. Pennings, "Optical multi-mode interference devices based on self-imaging: Principles and applications," *J. Lightwave Technol.* **13**, no. 4, 615–627, 1995.

8. F. A. Jenkins and H. E. White, *Fundamentals of Optics* (McGraw-Hill, Inc., New York, 1950).

9. R. Ulrich and G. Ankele, "Self-imaging in homogeneous planar optical waveguides," *Appl. Phys. Lett.* **27**, no. 6, 337–339, 1975.

10. R. Ulrich and T. Kamiya, "Resolution of self-images in planar optical waveguides," *J. Opt. Soc. Am.* **68**, no. 5, 583–592, 1978.

Distribution

Admnstr
Defns Techl Info Ctr
Attn DTIC-OCP
8725 John J Kingman Rd Ste 0944
FT Belvoir VA 22060-6218

Ofc of the Dir Rsrch and Engrg
Attn R Menz
Pentagon Rm 3E1089
Washington DC 20301-3080

Ofc of the Secy of Defns
Attn ODDRE (R&AT) G Singley
Attn ODDRE (R&AT) S Gontarek
The Pentagon
Washington DC 20301-3080

OSD
Attn OUSD(A&T)/ODDDR&E(R) R Tru
Washington DC 20301-7100

CECOM
Attn PM GPS COL S Young
FT Monmouth NJ 07703

CECOM RDEC Elect System Div Dir
Attn J Niemela
FT Monmouth NJ 07703

CECOM
Sp & Terrestrial Commctn Div
Attn AMSEL-RD-ST-MC-M H Soicher
FT Monmouth NJ 07703-5203

Dir of Assessment and Eval
Attn SARD-ZD H K Fallin Jr
103 Army Pentagon Rm 2E673
Washington DC 20301-0163

Hdqtrs Dept of the Army
Attn DAMO-FDT D Schmidt
400 Army Pentagon Rm 3C514
Washington DC 20301-0460

MICOM RDEC
Attn AMSMI-RD W C McCorkle
Redstone Arsenal AL 35898-5240

US Army Avn Rsrch, Dev, & Engrg Ctr
Attn T L House
4300 Goodfellow Blvd
St Louis MO 63120-1798

US Army CECIM
Attn AMSEL-RD-ST-ST-TE L A Coryell
FT Monmouth NJ 07703-5000

US Army CECOM Rsrch, Dev, & Engrg Ctr
Attn R F Giordano
FT Monmouth NJ 07703-5201

US Army CECOM Rsrch, Dev, & Engrg Ctr
Attn AMSEL-RD-ST-ST-TE J G Wright
FT Monmouth NJ 07703-5203

US Army Edgewood Rsrch, Dev, & Engrg Ctr
Attn SCBRD-TD J Vervier
Aberdeen Proving Ground MD 21010-5423

US Army Info Sys Engrg Cmnd
Attn ASQB-OTD F Jenia
FT Huachuca AZ 85613-5300

US Army Materiel Sys Analysis Agency
Attn AMXSY-D J McCarthy
Aberdeen Proving Ground MD 21005-5071

US Army Matl Cmnd
Dpty CG for RDE Hdqtrs
Attn AMCRD BG Beauchamp
5001 Eisenhower Ave
Alexandria VA 22333-0001

US Army Matl Cmnd
Prin Dpty for Acquisition Hdqrts
Attn AMCDCG-A D Adams
5001 Eisenhower Ave
Alexandria VA 22333-0001

US Army Matl Cmnd
Prin Dpty for Techlgy Hdqrts
Attn AMCDCG-T M Fisette
5001 Eisenhower Ave
Alexandria VA 22333-0001

US Army Natick Rsrch, Dev, & Engrg Ctr
Acting Techl Dir
Attn SSCNC-T P Brandler
Natick MA 01760-5002

US Army Rsrch Ofc
Attn G Iafrate
4300 S Miami Blvd
Research Triangle Park NC 27709

Distribution

US Army Simulation, Train, & Instrmntn
Cmnd
Attn J Stahl
12350 Research Parkway
Orlando FL 32826-3726

US Army Tank-Automtv & Armaments Cmnd
Attn AMSTA-AR-TD C Spinelli
Bldg 1
Picatinny Arsenal NJ 07806-5000

US Army Tank-Automtv Cmnd
Rsrch, Dev, & Engrg Ctr
Attn AMSTA-TA J Chapin
Warren MI 48397-5000

US Army Test & Eval Cmnd
Attn R G Pollard III
Aberdeen Proving Ground MD 21005-5055

US Army Train & Doctrine Cmnd
Battle Lab Integration & Techl Dirctrt
Attn ATCD-B J A Klevecz
FT Monroe VA 23651-5850

US Military Academy
Dept of Mathematical Sci
Attn MAJ D Engen
Attn MAJ B Sadowski
West Point NY 10996

USAASA
Attn MOAS-AI W Parron
9325 Gunston Rd Ste N319
FT Belvoir VA 22060-5582

Nav Surface Warfare Ctr
Attn Code B07 J Pennella
17320 Dahlgren Rd Bldg 1470 Rm 1101
Dahlgren VA 22448-5100

GPS Joint Prog Ofc Dir
Attn COL J Clay
2435 Vela Way Ste 1613
Los Angeles AFB CA 90245-5500

DARPA
Attn B Kaspar
Attn L Stotts
3701 N Fairfax Dr
Arlington VA 22203-1714

ARL Electromag Group
Attn Campus Mail Code F0250 A Tucker
University of Texas
Austin TX 78712

Texas Christian University Dept of Engrg
Attn T Tayag (10 copies)
TCU Box 298640
FT Worth TX 76129

University of Delaware
Dept of Elect & Comp Engrg
Attn D Prather
Newark DE 19716

University of Maryland E E Dept
Attn M D'Agenais
College Park MD 20742

University of Pittsburgh
Attn D Langer
Attn D-S Min
Attn H K Kim
348 Benedum Hall
Pittsburgh PA 15261

Boeing D&S Grp
Attn W Charczenko
PO Box 3999 MS 3W-51
Seattle WA 98124

Dir for MANPRINT
Ofc of the Deputy Chief of Staff for Prsnnl
Attn J Hiller
The Pentagon Rm 2C733
Washington DC 20301-0300

DRA Elec Div
Attn M Lewis
RSRE St Andrews Rd
Malvern Worcs WR14 #PS
UK

Fermionics Corp
Attn Y-Z Liu
4555 Runway Stret
Simi Valley CA 93063

Distribution

Palisades Instit for Rsrch Svc Inc
Attn E Carr
1745 Jefferson Davis Hwy Ste 500
Arlington VA 22202-3402

US Army Rsrch Lab
Attn AMSRL-CI-LL Techl Lib (3 copies)
Attn AMSRL-CS-AL-TA Mail & Records Mgmt
Attn AMSRL-CS-AL-TP Techl Pub (3 copies)
Attn AMSRL-SE D Wilmot
Attn AMSRL-SE J Mait
Attn AMSRL-SE J Pellegrino
Attn AMSRL-SE-EM B Riely
Attn AMSRL-SE-EM G Euliss
Attn AMSRL-SE-EM G Simonis
Attn AMSRL-SE-EM J Pamulapati
Attn AMSRL-SE-EM K Ritter
Attn AMSRL-SE-EM L Harrison
Attn AMSRL-SE-EM M Stead
Attn AMSRL-SE-EM P Shen
Attn AMSRL-SE-EM W Chang
Attn AMSRL-SE-EM W Zhou

US Army Rsrch Lab (cont'd)
Attn AMSRL-SE-EO A Mott
Attn AMSRL-SE-EO B Ketchel
Attn AMSRL-SE-EO B Zandi
Attn AMSRL-SE-EO C Heid
Attn AMSRL-SE-EO C Walker
Attn AMSRL-SE-EO D Chiu
Attn AMSRL-SE-EO D Mackie (10 copies)
Attn AMSRL-SE-EO D Morton
Attn AMSRL-SE-EO D Smith
Attn AMSRL-SE-EO G Daunt
Attn AMSRL-SE-EO G Wood
Attn AMSRL-SE-EO J Goff
Attn AMSRL-SE-EO J van der Gracht
Attn AMSRL-SE-EO K Bennett
Attn AMSRL-SE-EO M Miller
Attn AMSRL-SE-EO N Gupta
Attn AMSRL-SE-EO P Brody
Attn AMSRL-SE-EO R Dahmani
Attn AMSRL-SE-EO T Wong
Adelphi MD 20783-1197

REPORT DOCUMENTATION PAGE

Form Approved
OMB No. 0704-0188

1. AGENCY USE ONLY *(Leave blank)*	2. REPORT DATE	3. REPORT TYPE AND DATES COVERED
	February 1998	Final, from January 1996 to August 1996

4. TITLE AND SUBTITLE
A Technique to Ease the Fabrication Tolerance of Integrated Optical Power Splitters

5. FUNDING NUMBERS
PE: 62120A

6. AUTHOR(S)
Tristan J. Tayag (Texas Christian University) and David M. Mackie (ARL)

7. PERFORMING ORGANIZATION NAME(S) AND ADDRESS(ES)
U.S. Army Research Laboratory
Attn: AMSRL-SE-EO (email: dmackie@arl.mil)
2800 Powder Mill Road
Adelphi, MD 20783-1197

8. PERFORMING ORGANIZATION REPORT NUMBER
ARL-TR-1517

9. SPONSORING/MONITORING AGENCY NAME(S) AND ADDRESS(ES)
U.S. Army Research Laboratory
2800 Powder Mill Road
Adelphi, MD 20783-1197

10. SPONSORING/MONITORING AGENCY REPORT NUMBER

11. SUPPLEMENTARY NOTES
AMS code: 622120.H16
ARL PR: 6N0VT1

12a. DISTRIBUTION/AVAILABILITY STATEMENT
Approved for public release; distribution unlimited.

12b. DISTRIBUTION CODE

13. ABSTRACT *(Maximum 200 words)*

Fabrication tolerances and sidewall scattering losses in self-imaging waveguide devices are ameliorated by a partial-etch fabrication technique. Using a modal decomposition model, we find that the self-imaging plane's depth of focus increases with a reduction in etch depth. A broad depth of focus in the self-image plane relaxes the fabrication tolerance of the device's critical width dimension for a specified device performance. Trade-offs for this increased depth of focus include a modest increase in device length and a slight reduction in peak coupling efficiency.

14. SUBJECT TERMS
Talbot effect, integrated optics waveguides

15. NUMBER OF PAGES
19

16. PRICE CODE

17. SECURITY CLASSIFICATION OF REPORT	18. SECURITY CLASSIFICATION OF THIS PAGE	19. SECURITY CLASSIFICATION OF ABSTRACT	20. LIMITATION OF ABSTRACT
Unclassified	Unclassified	Unclassified	UL

NSN 7540-01-280-5500

Standard Form 298 (Rev. 2-89)
Prescribed by ANSI Std. Z39-18
298-102